

PAPER • OPEN ACCESS

Collective spin waves in RKKY interlayer-coupled $\text{Ni}_{80}\text{Fe}_{20}/\text{Ru}/\text{Ni}_{80}\text{Fe}_{20}$ nanowire arrays

To cite this article: Adekunle O Adeyeye *et al* 2024 *J. Phys.: Condens. Matter* **36** 395801

View the [article online](#) for updates and enhancements.

You may also like

- [Applications of nanomagnets as dynamical systems: II](#)
Bivas Rana, Amrit Kumar Mondal, Supriyo Bandyopadhyay *et al.*
- [Alkyl Dicarbonates, Common Electrolyte Degradation Products, Can Enable Long-Lived Li-Ion Cells at High Temperatures](#)
Tina Taskovic, Anu Adamson, Alison Clarke *et al.*
- [Experimental Study of Current Collection in Single-Chamber Micro Solid Oxide Fuel Cells with Combiike Electrodes](#)
Melanie Kuhn, Teko W. Napporn, Michel Meunier *et al.*

Collective spin waves in RKKY interlayer-coupled Ni₈₀Fe₂₀/Ru/Ni₈₀Fe₂₀ nanowire arrays

Adekunle O Adeyeye^{1,2,*} , Bushra Hussain³, Michael G Cottam⁴ 
and Gianluca Gubbiotti⁵ 

¹ Department of Physics, Durham University, South Rd, DH1 3LE Durham, United Kingdom

² Department of Electrical and Computer Engineering, National University of Singapore, 4 Engineering Drive 3, Singapore 117576, Singapore

³ Department of Natural Sciences, University of Michigan, Dearborn, MI 48128, United States of America

⁴ Department of Physics and Astronomy, University of Western Ontario, London, Ontario N6A 3K7, Canada

⁵ Cnr-Istituto Officina dei Materiali, Via Alessandro Pascoli, 06123 Perugia, Italy

E-mail: adekunle.o.adeyeye@durham.ac.uk

Received 2 March 2024, revised 11 June 2024

Accepted for publication 17 June 2024

Published 28 June 2024



Abstract

We report on a comprehensive investigation of collective spin waves in Ruderman–Kittel–Kasuya–Yosida (RKKY) interlayer-coupled Ni₈₀Fe₂₀ (10 nm)/Ru(1.0 nm)/Ni₈₀Fe₂₀ (10 nm) nanowire (NW) arrays. We employed Brillouin light scattering to probe the field- and wavevector-dependences of the spin-wave frequency spectra. The acquired data were subsequently analyzed and interpreted within the framework of a microscopic Hamiltonian-based method, enabling a detailed understanding of the observed spin-wave behavior. We observed the propagation of Bloch-type collective spin waves within the arrays, characterized by distinct magnonic bandwidths that stem from the combined influence of RKKY interlayer and inter-NW dynamical dipolar interactions.

Keywords: RKKY, spin waves, magnetic nanowires, Brillouin light scattering, interlayer exchange coupling, spin dynamics

1. Introduction

Magnetic nanowires (NWs) are prospective candidates for reprogrammable magnonic crystals, which could be useful in applications such as tuneable microwave band-pass and band-stop filters based on travelling spin waves [1, 2]. The knowledge of the band structure of magnonic crystals is an

important prerequisite for the successful design of spin-wave-based microwave devices. The experimental observations of tuneable band gaps in magnetic systems such as synthetic nanostructured magnonic crystals composed of two different magnetic materials [3] and magnetostatically coupled 1D NWs of the same magnetic material [4] are of significant interest. Theoretical studies have shown that multilayered NWs, where magnetic layers are coupled by exchange and/or dipolar interlayer interaction, can exhibit richer and more complex spin wave dispersion and magnonic band structures than single-layered ones [5]. The magnetostatic resonances of isolated (noninteracting) trilayered NiFe/Cu/NiFe NWs were studied both experimentally and theoretically as a function of the transverse wave vector (k) and of the intensity of an

* Author to whom any correspondence should be addressed.



Original content from this work may be used under the terms of the [Creative Commons Attribution 4.0 licence](https://creativecommons.org/licenses/by/4.0/). Any further distribution of this work must maintain attribution to the author(s) and the title of the work, journal citation and DOI.

external magnetic field applied along the NW long axis [6]. Due to the dipolar coupling between the NiFe layers, both acoustic and optical resonances were detected depending on whether the precession of the dynamic magnetization in the two NiFe layers is in-phase or out-of-phase, respectively. Later, the reprogrammability of the magnonic band structure for collective spin waves in dense arrays of NiFe/Cu/NiFe NWs was measured by Brillouin light scattering (BLS) and interpreted in terms of a Hamiltonian-based method. The frequency position of stationary and dispersive modes can be up- or down-shifted depending on the relative orientation of the magnetizations in the two NiFe layers [7]. It was shown that the magnetic modes are spin waves of the Bloch type propagating through the NW array with different magnonic bandwidths due to the interplay between the intra- and inter-NW dynamic dipolar interactions. A detailed understanding of the mode character, e.g. whether they have a stationary or propagating character, is achieved by considering the phase relation (either in-phase or out-of-phase) between the dynamic magnetizations in the two ferromagnetic (FM) layers and their average value over the NW stack [8].

The short-range interaction between two magnetic layers separated by a nonmagnetic metal layer, the interlayer exchange coupling (IEC), has been widely studied for its applications in magnetic memory devices [9, 10]. The IEC can oscillate between parallel and antiparallel alignments of the magnetic layers, depending on the thickness and material of the nonmagnetic spacer due to the Ruderman–Kittel–Kasuya–Yosida (RKKY) interaction, which has been exploited in a wide range of spintronic devices [11–14]. It was previously shown that when the spacer layer thickness is varied, the type of coupling switches between FM and antiferromagnetic (AFM) [15, 16]. The IEC influences the dynamic properties of the magnetic layers, which are essential for high-speed data processing. Therefore, it is vital to understand how the IEC affects the magnetization dynamics in trilayer structures. The IEC between the FM layers can change the band structure of layered nanostructures, affecting the central frequencies and width of the band gaps [17]. These are important factors for controlling spin-wave propagation, which is the basis of future high-speed information processing devices. Therefore, it is essential to understand how the IEC influences the dynamic responses of these nanostructures. It is known that other mechanisms such as biquadratic (BQ) exchange may also contribute to the IEC, and this possibility is briefly discussed later.

In this work, we investigate the collective spin waves in periodic arrays of Ni₈₀Fe₂₀/Ru/Ni₈₀Fe₂₀ NWs with Ru layer thickness of 1.0 nm in the presence of both interlayer RKKY interaction within one and the same NW and the long-range dipolar coupling within and between all NWs. The static behavior of the NW arrays was measured using the longitudinal magneto-optic Kerr effect (MOKE) with the magnetic field applied along the easy axis direction (i.e. along the wire length). The experimental spin-wave spectra were obtained by means of BLS that has demonstrated to be a very powerful tool for measuring the thermally excited SW properties FM thin and ultrathin films and multilayers [18, 19] and patterned structures [20, 21]. In the case of layered NWs, the interlayer

exchange coupling is determined by comparing the theoretical calculation with the field and wave-vector dependences of the spin-wave frequencies.

2. Experimental details

Periodic arrays of Ni₈₀Fe₂₀(10 nm)/Ru(1.0 nm)/Ni₈₀Fe₂₀(10 nm) trilayer NWs with length $l = 4$ mm, width $w = 400$ nm, separation of 70 nm and pitch $p = 470$ nm were fabricated on silicon substrates using deep ultraviolet lithography at 248 nm wavelength followed by a lift-off process [22]. The Ni₈₀Fe₂₀ (NiFe) and Ru layers were deposited using electron-beam evaporation and DC magnetron sputtering at 0.02 nm s⁻¹ and 0.005 nm s⁻¹, respectively, in a chamber with a base pressure lower than 2×10^{-8} Torr. The Ar working pressure during sputtering was 3 mTorr. The layered structure is fabricated in subsequent deposition steps of the NiFe and Ru layers without breaking the chamber's vacuum. A 5 nm thick Cr layer was deposited before the NiFe/Ru/NiFe multilayer for adhesion. We then used a scanning electron microscope (SEM) to check the lift-off process's completion and the NWs' dimensions. A representative SEM image of the NW array is presented in figure 1 and shows well-defined NW arrays with sharp edges and uniform separation.

The longitudinal hysteresis loops were measured by MOKE magnetometry at room temperature. The linearly polarized incident laser beam is focused on the sample surface at an angle of about 30 degrees, and a photoelastic modulator modulates the reflected light at a frequency of 50 Hz. Finally, the signal is fed into an AC photodiode detector and the measured intensity as a function of the applied field leads to a hysteresis loop. The laser spot is focused down to a spot size with a diameter of 100 μm so that the information about the NW reversal process is averaged over a large number of NW periods. Due to the finite penetration depth of light into metallic layers (10–20 nm), we assume that both NiFe layers are probed even if the topmost layer provides the large signal contribution. The external magnetic field, which was applied parallel to the sample plane and to the NW length (easy axis), varied between +85 and -85 mT. The corresponding hysteresis loops are shown later in figure 4.

BLS experiments from thermally excited spin waves were performed by focusing a monochromatic beam of p-polarized light of wavelength $\lambda = 532$ nm on the sample surface over an area of about 40 μm in diameter. The inelastically scattered light was analyzed in frequency using a (3 + 3)-pass tandem Fabry–Pérot interferometer [23]. The sample is mounted on a goniometer to allow rotation around the field direction, i.e. to vary the incidence angle of light (θ) in the presence of an external magnetic field applied parallel to the sample plane and the NW long axis (easy direction). We first measure the frequency dependence on the applied magnetic field strength with the angle of incidence of the light fixed at $\theta = 15$ degrees that, considering the in-plane SW wavenumber $k = (4\pi/\lambda) \sin \theta$ entering into the scattering process due to the conservation of in-plane momentum [19], corresponds to $k = 0.61 \times 10^7$ rad m⁻¹. Then, by changing the angle

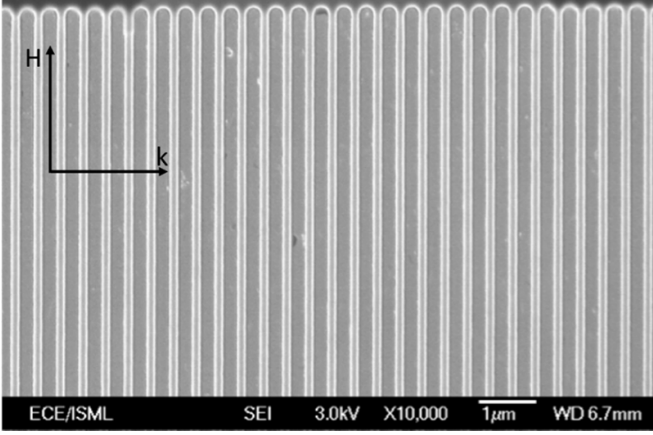


Figure 1. Scanning electron micrograph of the array of layered NWs. The directions of the applied magnetic field (H) and the spin-wave wave vector (k) are shown by the black arrows.

value, the spin-wave dispersion (frequency vs k) was measured by selecting the desired wave vector k along the transverse direction (perpendicular to the NW length) in the range between 0 and 2.0×10^7 rad m^{-1} in the presence of an applied field $\mu_0 H = 85$ mT that ensures the NWs saturation. Figure 2 shows the sequence of BLS spectra for different values of the external magnetic field. Three distinct peaks are observed over the entire field range investigated. Starting from the lowest frequency values these are labelled as 1, 2, and 3, as indicated for the spectrum measured at $\mu_0 H = 38$ mT. We notice that the central mode of this triplet, mode 2, has always the largest peak intensity over the entire field range investigated.

We note that the measured BLS spectra are noisy and peaks are rather broad, but from the inspection of both the Stokes and anti-Stokes sides, we can follow the evolution of the peak frequency as a function of the applied magnetic field (figure 4) and wave vector (figure 5). The error in the frequency values was estimated by fitting the experimental peaks by a Lorentzian curve after deconvolution with the transfer function of the interferometer with a typical width of 0.1 GHz. It was found that the error is comparable to the dimensions of the experimental points.

3. Theory

The theory is based on a microscopic approach in which we model the NiFe/Ru/NiFe NW as arrays of small cubic cells of effective spins, which can interact through the short-range exchange interaction within each stripe, through the long-range dipole–dipole interactions within each stripe and between stripes, and through the IEC. A Hamiltonian formalism is employed in which dipole–dipole terms are represented as discrete-lattice sums, rather than a macroscopic approach derived from Maxwell’s equations. Specifically, details of the method are given in [24] for single stripes and for cases where there are interfaces between films [25] or stripes [26]. The analysis presented here represents a generalization of results in

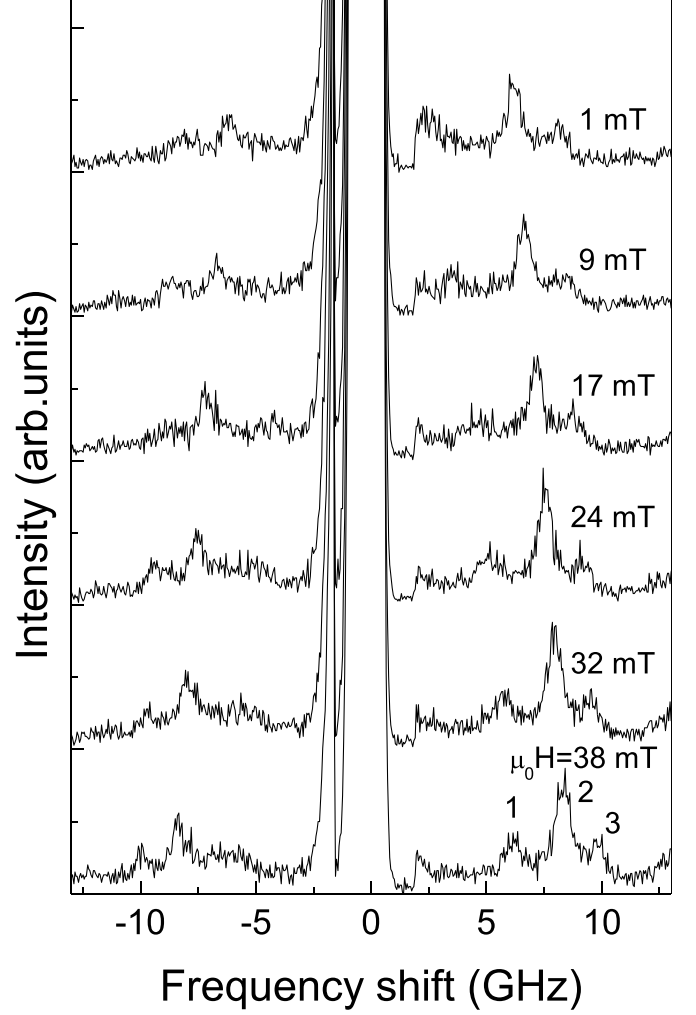


Figure 2. BLS spectra measured at $k = 0.61 \times 10^7$ rad m^{-1} for the NiFe/Ru/NiFe NWs array. The observed peaks are labelled as 1, 2, and 3 in the spectrum recorded at $\mu_0 H = 38$ mT. The external magnetic field is applied parallel to the NWs length and perpendicular to k (as shown in figure 1). The grey rectangular area covers the region of the elastic peak centred around zero frequency shift.

[26] to include the effects of *both* IEC and an interacting magnonic crystal array.

The geometry and choice of coordinate axes for the theoretical analysis are given schematically in figure 3. The vertical thicknesses of the NiFe stripes, which can be different in the theory, are denoted by d_1 and d_2 , and the smaller Ru thickness is t . The lateral width of the stripes is W and the lateral periodic length (or pitch) is p . Then the spin Hamiltonian can be expressed as

$$\mathcal{H} = -\frac{1}{2} \sum_{\mu, \mu'} \sum_{n, n'} J_{n\mu, n'\mu'} \mathbf{S}_{n\mu} \cdot \mathbf{S}_{n'\mu'} + \frac{1}{2} (g\mu_B)^2 \sum_{\mu, \mu'} \sum_{n, n'} \sum_{\alpha, \beta} D_{n\mu, n'\mu'}^{\alpha\beta} S_{n\mu}^\alpha S_{n'\mu'}^\beta - g\mu_B \mu_0 H \sum_{n\mu} S_{n\mu}^z \quad (1)$$

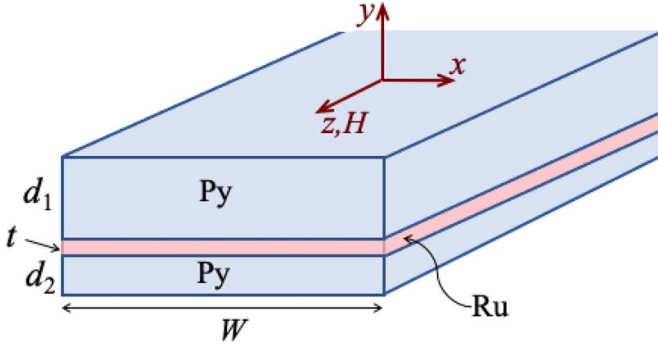


Figure 3. The geometry and choice of coordinate axes for just one of the NiFe/Ru/NiFe composite NWs in the magnonic crystal array. The applied magnetic field is along the length of the NiFe (or Py) stripes (z axis).

where $J_{n\mu, n'\mu'}$ is the total exchange interaction between the effective spins $\mathbf{S}_{n\mu}$ and $\mathbf{S}_{n'\mu'}$. Here the first index (n or n') labels the sites in any NW stripe, while indices μ and μ' ($= 1, 2, \dots, N_0$) label the stripes in the array. We will utilize the translational symmetry of the system along the longitudinal (or z) direction. The total number of spin sites in any cross section of the system (in the xy plane) is equal to $N_0 N$, where $N = W(d_1 + d_2)/a^2$ with a denoting the cell dimension. The usual criterion is that a should be chosen as less than the exchange correlation length of NiFe (which is of order 6 or 7 nm). In our modelling, we generally used an array of 21 NW stripes and $a = 5$ nm, which corresponds to ~ 6700 spin cells in a cross-section. Within any NiFe stripe the exchange interaction is taken to be nonzero (with value J) between nearest neighbours only and to be $-J_R$ due to RKKY interactions between closest sites across the Ru interface. The second term in \mathcal{H} is the contribution from the dipole–dipole interactions, where g is the Landé factor, μ_B is the Bohr magneton and

$$D_{n\mu, n'\mu'}^{\alpha\beta} = \frac{|\mathbf{r}_{n\mu, n'\mu'}|^2 \delta_{\alpha\beta} - 3r_{n\mu, n'\mu'}^\alpha r_{n\mu, n'\mu'}^\beta}{|\mathbf{r}_{n\mu, n'\mu'}|^5}. \quad (2)$$

Here $\alpha, \beta = x, y$ or z , and $\mathbf{r}_{n\mu, n'\mu'} = (x_n - x_{n'} + p[\mu - \mu'], y_n - y_{n'}, z_n - z_{n'})$ is the distance between spin sites in the array sample. Finally, equation (1) includes a term representing the Zeeman energy due to the applied field H .

Some additional terms that might optionally be included in the Hamiltonian are due to BQ exchange across the interface and single-ion anisotropies. These give rise to terms of the form $J_{n\mu, n'\mu'}^{\text{BQ}} (\mathbf{S}_{n\mu} \cdot \mathbf{S}_{n'\mu'})^2$ and $-K_{n\mu} (S_{n\mu}^z)^2$, respectively, which are summed over the relevant sites. The possible roles of these terms will be discussed in section 4.

The first stage of the calculation is to determine the equilibrium orientations of the N individual spins in any cross section. These change as the applied field H is varied, mainly due to its competing effects with the IEC and with the interlayer component of the dipole–dipole interactions. Briefly, we proceed as follows (see [24] for details). The spin operators $\mathbf{S}_{n\mu}$ appearing in the Hamiltonian are replaced by their mean-field averages $(\bar{S}_n^x, \bar{S}_n^y, \bar{S}_n^z)$, which are independent of the label μ and the z coordinate along a NW, to form an energy functional \bar{E} . An

iterative approach is then followed to find the actual spin components. For this, a trial starting configuration is assumed and the components $H_{\text{eff}}^\alpha(n)$ of the total effective field at each site in the cross section is obtained using the functional derivative $g\mu_B\mu_0 H_{\text{eff}}^\alpha(n) = -\delta\bar{E}/\delta\bar{S}_n^\alpha$. Each spin can then be re-oriented along the direction of its effective field, and the process can be continued in numerical iteration until convergence (typically 3×10^4 iterations is sufficient in the present case). In practice, several starting configurations are used to avoid local minima in \bar{E} .

Next, the SW modes are studied, following [24, 25], by transforming the Hamiltonian in equation (1) from the original $\{x, y, z\}$ global axes to new local axes $\{X, Y, Z\}$ for each spin, so that the new Z axis in each case is parallel to that spin orientation. A Holstein–Primakoff transformation [27] from spin operators to boson operators is made relative to the *new* axes, allowing an expansion to be made as $\mathcal{H} = \mathcal{H}^{(0)} + \mathcal{H}^{(1)} + \mathcal{H}^{(2)} + \dots$, where a general term $\mathcal{H}^{(s)}$ involves a product of s boson operators. The first term $\mathcal{H}^{(0)}$ is just a constant, while the next term $\mathcal{H}^{(1)}$ vanishes by symmetry due to the transformation of axes, leaving

$$\mathcal{H}^{(2)} = \sum_{n, m, k} A_{nm}(k) a_{kn}^\dagger a_{km} + B_{nm}(k) a_{kn}^\dagger a_{-kn}^\dagger + B_{nm}^*(k) a_{-kn} a_{km} \quad (3)$$

as the leading order term describing the SWs. The higher-order terms correspond to nonlinear SW processes, which are ignored here. In equation (3) we have a_{kn}^\dagger and a_{km} as the boson creation and annihilation operators, respectively, at sites n and m . Two wave-vector Fourier transforms have been made: along z (where there is longitudinal translational symmetry) and along x (where there is a Bloch wave vector due to the periodic array). We have simplified by setting the longitudinal wave vector to zero (as in the experiment) and k denotes the Bloch wave vector for the periodic system. The boundaries of the mini-Brillouin zone occur at multiples of π/p , where p is the pitch (or periodic length). The quantities $A_{nm}(k)$ and $B_{nm}(k)$ may be regarded as the matrix elements of the $N \times N$ matrices denoted as $\mathbf{A}(k)$ and $\mathbf{B}(k)$; they are deduced in terms of the parameters of the Hamiltonian in equation (1) and the equilibrium orientations, as described in [26].

As in related previous work, there are two results that follow from equation (4). One is that it may be ‘diagonalized’ using a linear canonical transformation (a Bogoliubov transformation) to a new set of boson operators $\{b_{kl}\}$ such that

$$\mathcal{H}^{(2)} = \sum_{k, l} \hbar\omega_{kl} b_{kl}^\dagger b_{kl} \quad (4)$$

where $l (= 1, 2, \dots, N)$ is a mode number and ω_{kl} is the corresponding SW frequency. The other useful result is that we can form a $2N \times 2N$ dynamical matrix by

$$\begin{pmatrix} \mathbf{A}(k) & 2\mathbf{B}(k) \\ -2\mathbf{B}^*(-k) & -\tilde{\mathbf{A}}(-k) \end{pmatrix}. \quad (5)$$

It has the property that its N positive eigenvalues are just the SW frequencies ω_{kl} and the corresponding eigenvectors

provide information about the SW amplitudes at different sites (including the relative phases). We would like to specify that, the dynamic magnetizations in adjacent NWs are related by the Bloch theorem, namely $m(x \pm np) = m(x)e^{\pm iknp}$ where n is a positive integer number and p is the array periodicity. Since the observed modes are standing spin-wave resonating through the NW width, the shape of the mode profiles is independent of the wavevector value which, contrarily, introduces a phase relation between the oscillating magnetization between the adjacent NWs and the frequency ordering of modes changes with the wavevector, i.e. the order of the modes (in ascending frequency) depends on k .

Moreover, we want to remark that we included BQ inter-layer exchange interaction in our theory, but it gave no improvement on the fit of the experimental frequencies probably because it is negligible when compared to the RKKY interaction. In past work, BQ effects were found to be negligible for complete films [25]. By contrast the BQ effects were important for small-width NWs [26]. In the present study, we have fairly wide NWs, so the conclusion of negligible BQ effects seems consistent.

4. Experimental results and discussion

In figure 4 we show the MOKE hysteresis loops and the BLS frequency evolution as a function of the external magnetic field applied along the NW length within the same field range for the sample investigated. A small remanence characterizes the MOKE loops for the sample, and a saturation that is reached gradually indicates an AFM coupling between the NiFe layers. The M - H loop shows a gradual change of net magnetization followed by an almost flat region with zero net magnetization at remanence. This indicates the transition from the spin-flop (SF) phase to an AFM state where the magnetizations in the two NiFe layers point in opposite directions.

This behavior is different from what was previously measured in dipolar coupled NiFe/Cu/NiFe NWs in the presence of a 10 nm thick Cu spacer, where the magnetization curves measured by MOKE reveal the presence of a double-step hysteresis loops associated with the different switching fields of the two permalloy layers [7].

Regarding the BLS frequency measurements, figure 4 displays the measured frequencies plotted as a function of the applied field magnitude. Starting from positive saturation with $H = +85$ mT, the field is decreased in magnitude down to zero and then reversed to negative values toward negative saturation following the descending branch of the hysteresis loops. The lowest frequency mode (1) has essentially a linear frequency dependence on the applied field in the high field range; a frequency downshift and a nonlinear dependence are observed below about 25 mT. This deviation occurs at the same field where the magnetization starts to reduce from the saturation value. Contrarily, the frequencies of modes (2) and (3) always present an almost linear dependence with H .

The (blue) continuous and dashed curves are the theoretical frequencies calculated using the theory described in section 3. The continuous curves represent modes having the largest BLS

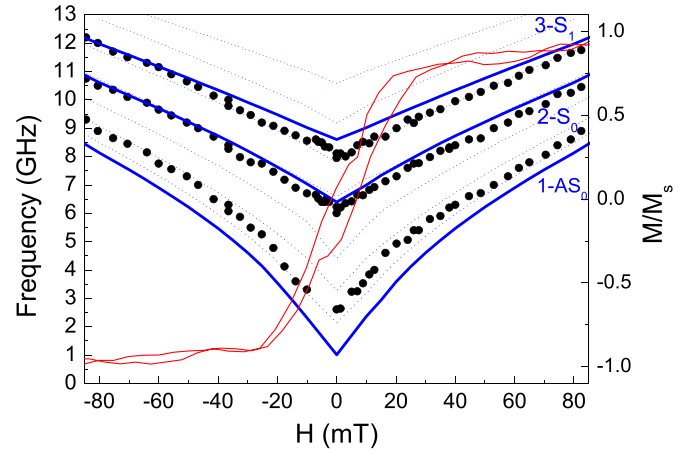


Figure 4. Field evolution of the measured (black points) and calculated (blue lines) eigenmode frequency of NiFe/Ru/NiFe NWs array. The solid blue lines represent the most intense modes. We associate with each BLS peak (1, 2 and 3) the corresponding calculated spatial profile, symmetric (S) and asymmetric (AS), shown in figure 6. The normalized MOKE hysteresis loops (red curve) are also plotted for comparison with the BLS results.

cross-section to be compared with the experimental BLS peak frequencies while the dashed curves represent those modes with negligible intensity.

An overall good agreement between experimental and calculated frequencies is obtained over the entire field range investigated especially for peaks 2 and 3. For peak 1 the qualitative dependence on H is well reproduced by theory, but the calculated frequency of this mode is underestimated slightly. The reason for this is unclear, but possibly it is an indication that the uniaxial anisotropy field in the NiFe layers depends on position within the sample (e.g. it might be different at the lateral edges compared with the interior of the sample). The parameter values used for NiFe in the theory are well known from previous experimental work (e.g. [25, 26]), comprising the exchange stiffness $\mathcal{D} = 30$ T, the saturation magnetization $M_s = 0.071$ T nm², and the gyromagnetic ratio with $g\mu_B = 29.3$ GHz T⁻¹. They can all be related back to the parameters in the original spin Hamiltonian in equation (1). For the cubic cell size, we generally assumed $a = 5$ nm, although smaller sizes were also used as a check on consistency. The inclusion of nonzero uniaxial anisotropy K gave a marginal improvement in fit. We used $SK/g\mu_B = 0.01$ T at all spin sites for simplicity. These values are comparable to those used in previous studies for NiFe NWs.

To understand whether the detected modes have a stationary or propagating behavior through the NW array, we measure the SW dispersion by sweeping the wave vector k in the transverse direction of the NWs. Figure 5 shows the comparison between the measured and the calculated SW dispersion (frequency vs Bloch wavenumber k) within the first Brillouin zone for NW arrays with different Ru thicknesses in the saturated state ($\mu_0 H = 85$ mT). The lowest-frequency mode is dispersionless, i.e. its frequency does not change as a function of the k , while the second lowest-frequency mode exhibits a significant magnonic bandwidth of about 1.6 GHz. When

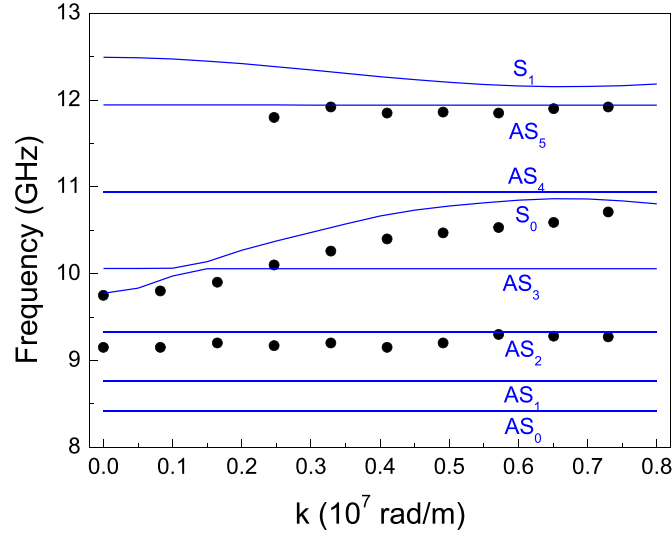


Figure 5. Comparison between the measured and calculated spin-wave band structure in the first Brillouin zone of the array for the NiFe/Ru/NiFe NWs array. The external magnetic field is $\mu_0 H = 85$ mT applied parallel to the NW length. We label each calculated mode as symmetric (S) and asymmetric (AS) while the integer number defines the number of mode nodes across the NW width.

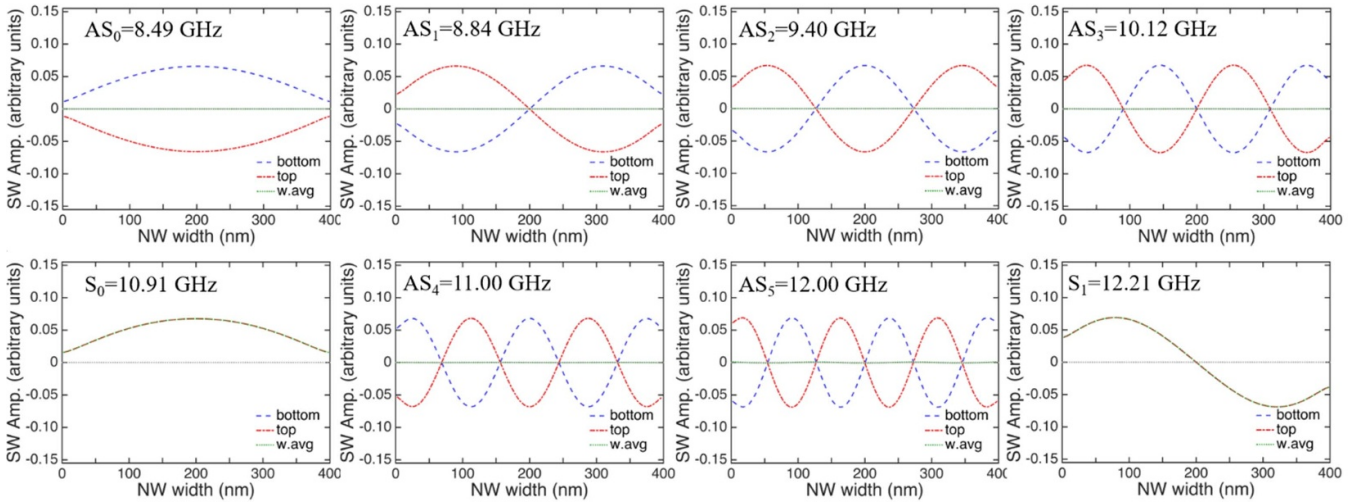


Figure 6. Spatial distribution (real part of in-plane x -component) of the eight lowest-frequency modes for the NiFe/Cu/NiFe NWs. The magnetic field $H = +85$ mT is applied along the NW length and k is fixed at 0.61×10^7 rad m^{-1} . The blue and red curves refer to the bottom and top NiFe layers, respectively while the green curves are the average values of the dynamic magnetization across the two layers. The modes are labelled as S (symmetric) and AS (anti-symmetric).

explored beyond the edge of the first BZ, which occurs at $k_{BZ} = \pi/p \sim 0.69 \times 10^7$ rad m^{-1} , the SW dispersion exhibits the characteristic periodic behavior of the Bloch-type collective spin waves, which is caused by the artificial periodicity of the lattice. A third mode with stationary behavior is observed at about 12 GHz. Even in this case, the calculated frequency dispersion reproduces very well the experimental results over the entire wave-vector range investigated. Finally, the RKKY coupling parameter $-J_R$ is deduced from the best fit to the experimental BLS data, leading to an approximate value for the ratio J_R/J of 0.002, which is consistent with previous NiFe/Ru/NiFe studies for a Ru thickness of 1.0 nm [26].

In order to interpret the measured dispersion of figure 5 and the field dependent results of figure 4, we calculated the spatial

profile of the modes across the NW width and considered the phase difference between the precessing magnetization vectors in the two NiFe layers. In figure 6 we show the real part of in-plane x -component of the eight lowest-frequency modes calculated for $\mu_0 H = +85$ mT is applied along the NW length and k fixed at 0.61×10^7 rad m^{-1} . Since the two layers are coupled by both the RKKY and dipolar interactions, the resonance modes can be classified as symmetric (S) and anti-symmetric (AS) modes depending on whether the oscillation in the two layers is in-phase or anti-phase. In all cases, the mode profiles have a sinusoidal shape and are characterized by an increasing number of nodes across the NW width. The four modes with the lowest frequency belong to the family of AS modes. The first one (AS_0), which is characterized by a nearly

uniform precession amplitude across the width of the NWs, can be considered as a quasi-uniform (fundamental) mode of the NWs, while the other three asymmetric modes have an increasing number of nodes across the NW width and exhibit a non-dispersive behavior, i.e. their frequency is constant as a function of the wave vector k . Mode S_0 exhibits the largest intensity peak and it associated to peak 2 in the measured BLS spectra because of its symmetric character and the non-zero averaged dynamic magnetization. This mode also has the largest magnonic bandwidth due to that efficient dipolar coupling between neighbouring NWs, which gives rise to collective SWs of the Bloch type travelling on the periodic array. It is worth mentioning, that while the anti-symmetric modes (AS) should have a zero BLS cross-section due to zero averaged dynamic magnetization, they could have a non-zero intensity due to the finite penetration depth of light that mostly illuminates the uppermost layer and to finite wave vector k . These two aspects are responsible for the fact that lowest frequency asymmetric modes, such as mode AS_0 , gives a non-vanishing contribution to the BLS cross-section (see equation (1) of [28]) and it is associated to peak 1 in figures 2 and 3. Using similar considerations, we have assigned to each experimental BLS peak 3 the label corresponding to the calculated spatial profile of mode S_1 .

Although both the RKKY interactions and the dipole-dipole interactions provide coupling between the NiFe layers, our conclusion is that the former play the dominant overall role for the spin-wave dynamics in this system. Qualitatively, they give rise to different effects since the RKKY interactions are short range and act in the vertical (y) direction. By contrast, the long-range dipolar interactions give coupling in all directions including between NW array elements extending along the x direction.

5. Conclusions

We have presented a comprehensive study of the spin-wave modes in a magnonic crystal fabricated as a lateral array of trilayer NiFe/Ru/NiFe NWs. The system was characterized by MOKE magnetometry and the collective spin-wave excitations were detected by BLS spectroscopy. A microscopic (or Hamiltonian-based) theoretical method was employed to calculate the dependence of spin-wave frequencies and amplitudes (including relative phase) on the longitudinal applied magnetic field and the transverse (or Bloch) wave vector. Overall, the agreement between theory and experiment was found to be good. Particular attention was given to the role of the IEC in any NW provided by short-range RKKY interaction in the vertical (y) direction. The coupling between the NWs in the lateral (x) direction arises due to the long-range dipole-dipole interactions, giving rise to the magnonic bands of the array.

We believe that the results of this work are interesting for future applications in the field of three-dimensional magnonics, where the spin-wave properties can be controlled by the interplay of RKKY and dipole interactions between the layers.

Data availability statement

The data that support the findings of this study are openly available at the following URL/DOI: <https://zenodo.org/doi/10.5281/zenodo.10618696>.

Acknowledgments

This project received funding from the European Union's Horizon 2020 Research and Innovation Program under Grant Agreement No. 101007417 having benefited from the IOM-CNR access provider in the Perugia access site within the framework of the NFFA-Europe Pilot Transnational Access Activity, Proposal No. ID 322.

A O A and G G acknowledge the funding from the Royal Society through the Wolfson Fellowship and International Exchanges IEC\R2\222074. NSERC.

This work has been supported by the European Union—Next Generation EU under the Italian Ministry of University and Research (MUR) National Innovation Ecosystem grant ECS00000041—VITALITY. CUP: B43C22000470005.

Drs Navab Singh and Lulu Xiong are thanked for the DUV templates and sample fabrication.

ORCID iDs

Adekunle O Adeyeye  <https://orcid.org/0000-0001-9724-2468>

Michael G Cottam  <https://orcid.org/0000-0002-7775-0083>

Gianluca Gubbiotti  <https://orcid.org/0000-0002-7006-0370>

References

- [1] Lenk B, Ulrichs H, Garbs F and Müntenberg M 2011 The building blocks of magnonics *Phys. Rep.* **507** 107
- [2] Barman A et al 2021 The 2021 magnonics roadmap *J. Phys.: Condens. Matter* **33** 413001
- [3] Wang Z K, Zhang V L, Lim H S, Ng S C, Kuok M H, Jain S and Adeyeye A O 2009 Observation of frequency band gaps in a one-dimensional nanostructured magnonic crystal *Appl. Phys. Lett.* **94** 083112
- [4] Gubbiotti G, Tacchi S, Madami M, Carlotti G, Adeyeye A O and Kostylev M 2010 Brillouin light scattering studies of planar metallic magnonic crystals *J. Phys. D: Appl. Phys.* **43** 264003
- [5] Mamica S, Krawczyk M, Sokolovskyy M L and Romero-Vivas J 2012 Large magnonic band gaps and spectra evolution in three-dimensional magnonic crystals based on magnetoferritin nanoparticles *Phys. Rev. B* **86** 144402
- [6] Gubbiotti G, Kostylev M, Sergeeva N, Conti M, Carlotti G, Ono T, Slavin A N and Stashkevich A 2004 Brillouin light scattering investigation of magnetostatic modes in symmetric and asymmetric NiFe/Cu/NiFe trilayered wires *Phys. Rev. B* **70** 224422
- [7] Gubbiotti G, Zhou X, Haghshenasfard Z, Cottam M G and Adeyeye A O 2018 Reprogrammable magnonic band

- structure of layered permalloy/Cu/permalloy nanowires *Phys. Rev. B* **97** 134428
- [8] Gubbiotti G, Zhou X, Haghshenasfard Z, Cottam M G, Adeyeye A O and Kostylev M 2019 Interplay between intra- and inter-nanowires dynamic dipolar interactions in the spin wave band structure of Py/Cu/Py nanowires *Sci. Rep.* **9** 4617
- [9] Vohl M, Barnas J and Grunberg P 1989 Effect of interlayer exchange coupling on spin-wave spectra in magnetic double layers: theory and experiment *Phys. Rev. B* **39** 12003
- [10] Maccio M, Pini M G, Politi P and Rettori A 1994 Spin-wave study of the magnetic excitations in sandwich structures coupled by bilinear and biquadratic interlayer exchange *Phys. Rev. B* **49** 3283
- [11] Wolf S A, Awschalom D D, Buhrman R A, Daughton J M, von Molnár S, Roukes M L, Chtchelkanova A Y and Treger D M 2001 Spintronics: a spin-based electronics vision for the future *Science* **294** 1488
- [12] Inomata K, Nozaki T, Tezuka N and Sugimoto S 2002 Magnetic switching field and giant magnetoresistance effect of multilayers with synthetic antiferromagnet free layers *Appl. Phys. Lett.* **81** 310
- [13] Nozaki T, Jiang Y, Kaneko Y, Hirohata A, Tezuka N, Sugimoto S and Inomata K 2004 Spin-dependent quantum oscillations in magnetic tunnel junctions with Ru quantum wells *Phys. Rev. B* **70** 172401
- [14] Lee K, Chen W-C, Zhu X, Li X and Kang S H 2009 Effect of interlayer coupling in CoFeB/Ta/NiFe free layers on the critical switching current of MgO-based magnetic tunnel junctions *J. Appl. Phys.* **106** 024513
- [15] Parkin S S P, More N and Roche K P 1990 Oscillations in exchange coupling and magnetoresistance in metallic superlattice structures: Co/Ru, Co/Cr, and Fe/Cr *Phys. Rev. Lett.* **64** 2304
- [16] Baibich M N, Broto J M, Fert A, Van Dau F N, Petroff F, Etienne P, Creuzet G, Friederich A and Chazelas J 1988 Giant magnetoresistance of (001)Fe/(001)Cr magnetic superlattices *Phys. Rev. Lett.* **61** 2472
- [17] Liu X M, Lupo P, Cottam M G and Adeyeye A O 2015 Tuning of interlayer exchange coupling in Ni₈₀Fe₂₀/Ru/Ni₈₀Fe₂₀ nanowires *J. Appl. Phys.* **118** 113902
- [18] Hillebrands B, Baumgart P and Güntherodt G 1989 Brillouin light scattering from spin waves in magnetic layers and multilayers *Appl. Phys. A* **49** 589
- [19] Demokritov S and Tsymbal E I 1994 Light scattering from spin waves in thin films and layered systems *J. Phys.* **6** 7145
- [20] Demokritov S O, Hillebrands B and Slavin A N 2001 Brillouin light scattering studies of confined spin waves: linear and nonlinear confinement *Phys. Rep.* **348** 441
- [21] Yoshihara A 2023 Brillouin light scattering from magnetic excitations *Materials* **16** 1038
- [22] Adeyeye A O and Singh N 2008 Large area patterned magnetic nanostructures *J. Phys. D: Appl. Phys.* **41** 153001
- [23] Sandercock J R 1982 *Light Scattering in Solids III* ed M Cardona and G Güntherodt (Springer) p 173
- [24] Nguyen H T, Nguyen T M and Cottam M G 2007 Dipole-exchange spin waves in ferromagnetic stripes with inhomogeneous magnetization *Phys. Rev. B* **76** 134413
- [25] Liu X M, Nguyen H T, Ding J, Cottam M G and Adeyeye A O 2014 Interlayer coupling in Ni₈₀Fe₂₀/Ru/Ni₈₀Fe₂₀ multilayer films: ferromagnetic resonance experiments and theory *Phys. Rev. B* **90** 064428
- [26] Lupo P, Haghshenasfard Z, Cottam M G and Adeyeye A O 2016 Ferromagnetic resonance study of interface coupling for spin waves in narrow NiFe/Ru/NiFe multilayer nanowires *Phys. Rev. B* **94** 214431
- [27] Holstein T and Primakoff H 1940 Field dependence of the intrinsic domain magnetization of a ferromagnet *Phys. Rev.* **58** 1098
- [28] Gubbiotti G, Carlotti G, Okuno T, Grimsditch M, Giovannini L, Montoncello F and Nizzoli F 2005 Spin dynamics in thin nanometric elliptical Permalloy dots: a Brillouin light scattering investigation as a function of dot eccentricity *Phys. Rev. B* **72** 184419